A&A 581, A38 (2015)
DOI: 10.1051/0004-6361/201526329

Astronomy & Astrophysics

The SOPHIE search for northern extrasolar planets

VII. A warm Neptune orbiting HD 164595⋆,⋆⋆

B. Courcol[1], F. Bouchy[1], F. Pepe[2], A. Santerne[3], X. Delfosse[4,10], L. Arnold[6], N. Astudillo-Defru[4,10], I. Boisse[1], X. Bonfils[4,10], S. Borgniet[4], V. Bourrier[2], N. Cabrera[4,10], M. Deleuil[1], O. Demangeon[1], R. F. Díaz[1,2], D. Ehrenreich[2], T. Forveille[4,10], G. Hébrard[5,6], A. M. Lagrange[4], G. Montagnier[5,6], C. Moutou[1,8], J. Rey[2], N. C. Santos[3,7], D. Ségransan[2], S. Udry[2], and P. A. Wilson[5,9]

[1] Aix Marseille Université, CNRS, Laboratoire d'Astrophysique de Marseille UMR 7326, 13388 Marseille Cedex 13, France
e-mail: bastien.courcol@lam.fr
[2] Département d'Astronomie de l'Université de Genève, 51 ch. des Maillettes – Sauverny, 1290 Versoix, Switzerland
[3] Instituto de Astrofísica e Ciências do Espaço, Universidade do Porto, CAUP, Rua das Estrelas, 4150-762 Porto, Portugal
[4] Univ. Grenoble Alpes, IPAG, 38000 Grenoble, France
[5] Institut d'Astrophysique de Paris, UMR 7095 CNRS, Université Pierre & Marie Curie, 98bis boulevard Arago, 75014 Paris, France
[6] Aix Marseille Université, CNRS, OHP, Institut Pythéas UMS 3470, 04870 Saint-Michel-l'Observatoire, France
[7] Departamento de Física e Astronomia, Faculdade de Ciências, Universidade do Porto, 4169-007 Porto, Portugal
[8] CFHT, 65-1238 Mamalahoa Hwy, 96743 Kamuela HI, USA
[9] Sorbonne Université, UPMC Univ Paris 06, UMR 7095, Institut d'Astrophysique de Paris, 75014 Paris, France
[10] CNRS, IPAG, 38000 Grenoble, France

Received 16 April 2015 / Accepted 12 June 2015

ABSTRACT

High-precision radial velocity surveys explore the population of low-mass exoplanets orbiting bright stars. This allows accurately deriving their orbital parameters such as their occurrence rate and the statistical distribution of their properties. Based on this, models of planetary formation and evolution can be constrained. The SOPHIE spectrograph has been continuously improved in past years, and thanks to an appropriate correction of systematic instrumental drift, it is now reaching 2 m s^{-1} precision in radial velocity measurements on all timescales. As part of a dedicated radial velocity survey devoted to search for low-mass planets around a sample of 190 bright solar-type stars in the northern hemisphere, we report the detection of a warm Neptune with a minimum mass of 16.1 ± 2.7 $M_\oplus$ orbiting the solar analog HD 164595 in 40 ± 0.24 days. We also revised the parameters of the multiplanetary system around HD 190360. We discuss this new detection in the context of the upcoming space mission CHEOPS, which is devoted to a transit search of bright stars harboring known exoplanets.

Key words. planetary systems – techniques: radial velocities – stars: individual: HD 164595 – stars: individual: HD 190360 – stars: individual: HD 185144

1. Introduction

Over the past 20 years, the radial velocity (RV) technique has benefited from continuous developments. Several major milestones in detection and characterization of extrasolar planets have been made possible with this technique, either in the context of large surveys or in follow-ups of transiting candidates. These developments allowed a few stabilized spectrographs like HARPS (Mayor et al. 2003) to gradually scan the area of Neptune-like objects and super-Earths and detect exoplanets with minimum masses as low as 1 $M_\oplus$ (Dumusque et al. 2012).

Recent exoplanet RV surveys show that over 40% of non-active solar-type stars probably harbor low-mass exoplanets (Mayor et al. 2011; Howard et al. 2010) with a mass distribution that seems to increase sharply toward low masses. In addition, most of the low-mass exoplanets belong to multiple compact systems (e.g., Lovis et al. 2011b). These results overall agree with the observed properties of the transiting exoplanets detected by the *Kepler* mission (Borucki & Koch 2011; Howard et al. 2012; Marcy et al. 2014). Detection and characterization of new low-mass exoplanets orbiting bright stars is motivated by the need to obtain accurate measurements of the projected mass and the eccentricity and to identify all the components of multiple systems to constrain models of exoplanet evolution. Such exoplanets orbiting bright stars will also be key targets for a deeper and more extended characterization with CHEOPS (Broeg et al. 2013; Fortier et al. 2014), for instance, which searches for the transit, and JWST (Beichman et al. 2014), which searches for atmospheric signatures.

The SOPHIE spectrograph (Perruchot et al. 2008) on the 1.93 m telescope of the Observatoire de Haute-Provence was improved in June 2011 with the implementation of octagonal-section fibers (Perruchot et al. 2011). This optimization led to an improvement in RV precision to nearly 2 m s^{-1} (Bouchy et al. 2013) on timescales of a few tens of days. This precision level is critical for detecting low-mass exoplanets around

⋆ Based on observations made with SOPHIE spectrograph on the 1.93-m telescope at Observatoire de Haute-Provence (CNRS/OSU Pythéas), France (program 07A.PNP.CONS).

⋆⋆ Appendix A is available in electronic form at http://www.aanda.org solar-type stars. In the context of the subprogram "High precision search for Neptunes and super-Earths" of the SOPHIE extrasolar planets research consortium (Bouchy et al. 2009), we redefined a sample of 190 bright stars on the following criteria: 1) in the northern hemisphere; 2) with spectral type G and K and $0.6 \leq B - V \leq 1.4$; 3) on a volume limited to 35 pc; 4) non-active ($v \sin i \leq 4.5$ km s^{-1}, $\log R'_{\rm HK} \leq -4.8$); 5) not part of a binary system and not harboring giant planets at short orbital period; and 6) not part of RV surveys carried out with HARPS-N GTO (Cosentino et al. 2012) at the TNG. This subprogram is intensively conducted since June of 2011.

We here report on the detection of a Neptune-like exoplanet candidate orbiting the solar analog HD 164595. Section 2 describes the SOPHIE observations and the data reduction. In Sect. 3 we describe the correction of the systematic instrumental drift necessary to reach the 2 m s^{-1} precision level. This correction is then validated in Sect. 4 using the known planetary system HD 190360, for which we provide an updated orbital solution. Section 5 details our data analysis of HD 164595 and summarizes the orbital and physical properties of the planet. We finally present our conclusions in Sect. 6.

2. Observations and data reduction

Spectroscopic observations were conducted with the SOPHIE spectrograph (Perruchot et al. 2008, 2011). SOPHIE is a fiber-fed environmentally stabilized echelle spectrograph covering the visible range from 387 to 694 nm. We used the high-resolution (HR) mode ($\lambda/\Delta\lambda = 75\,000$) with thorium-argon simultaneous wavelength calibration on fiber B.

In total we gathered 75 measurements of HD 164595 with SOPHIE over 2.2 years. The exposure time was set to between 800 and 1200 s to reach a signal-to-noise ratio (S/N) of 140 at typical photon-noise RV uncertainties below 1.0 m s^{-1} while simultaneously averaging p-mode stellar oscillations. Taking into account the wavelength calibration uncertainty (close to 1.0 m s^{-1}), the average RV uncertainty is 1.43 m s^{-1}. Nine spectra were identified as low quality. One measurement has a S/N that is half of the average, indicating a strong atmospheric absorption. Three measurements are affected by moon light contamination, which cannot be corrected with the simultaneous thorium mode. Five measurements present a flux anomaly of the thorium lamp, which prevented us from computing the simultaneous drift. They were discarded for the data analysis in Sect. 4.4.

The spectra were reduced and extracted using the SOPHIE pipeline (Bouchy et al. 2009), and the resulting wavelength-calibrated 2D spectra were correlated using a numerical binary mask corresponding to spectral type G2 to obtain the radial velocity measurement (Baranne et al. 1996; Pepe et al. 2002). The full width at half maximum (FWHM), contrast, and bisector span of the cross-correlation function (CCF) are also provided by the pipeline.

The complete radial velocity dataset, after the zero-point drift correction described in the next section, is reported in the Appendix and plotted in Fig. 8.

3. Correction of the systematic instrumental drift

Despite a clear improvement in RV precision provided by the implementation of octogonal fibers on timescales of a few tens of days (Bouchy et al. 2013; Perruchot et al. 2011), we identified long-term variations of the zero point of the instrument that added up to about ±10 m s^{-1} over the last 3.5 years (cf. Fig. 1, upper panel). The first ramp seems to be correlated with the thorium-argon lamp aging. One jump of about −7 m/s is related to the implementation of additional octagonal fibers after the double scrambling in December 2012 (BJD = 55 950). A second jump of −7 m/s at BJD = 56 775 appears after the coating of the secondary mirror of the 1.93 m telescope, which introduced a significant change in the flux balance across the spectral range. Other events, with a timescale of a few weeks, are clearly correlated with strong changes of the outside temperature, which are propagated to the tripod of the spectrograph at a level of a few tenths of degrees through the telescope pillar. A thermal control loop of the spectrograph tripod is under development to avoid such thermal conduction coming from the telescope pillar.

To track this long-term zero-point drift of the instrument, we systematically monitored a set of RV constant stars each night, namely HD 185144 (Howard et al. 2010), HD 9407, HD 221354, and HD 89269A (Howard et al. 2011), which were monitored with HIRES on the 10.2 m Keck telescope with an RV dispersion of 2.0, 1.7, 1.9, and 2.0 m s^{-1}, respectively, over several years. In addition to this set of four RV constant stars, we also used 51 targets from our sample that have at least ten measurements. We recursively built an RV constant master using these two sets of stars. A first master was created using a running median on the four reliable constant stars. This master was then subtracted from the second group, and all the stars with a corrected root mean square (rms) lower than a threshold of 3 m s^{-1} were included in the first subset. The offset for each star was adjusted as well to minimize the dispersion of the residuals. A double weight was given to the four reliable constant stars. This process was repeated until convergence, that is, when no additional star was added to the first subset.

The running median was implemented with the criterium to average 15 measurements. This was preferred instead of taking a fixed time window to give the same weight to all correction points. Consequently, a period with a higher density of observations will increase the temporal resolution of the correction. On the other hand, a period with sparse measurements will lead to a lower temporal resolution instead of a poorer constraint on the correction point. In practice, with this criteria of 15 measurements averaged, the typical timescale of the correction is nine days.

The most satisfying correction uses a threshold of 3 m s^{-1} and converges after four iterations with a total of 23 constant stars in the final set. The radial velocities of these 23 constant stars as well as the derived RV constant master[1] are displayed in the top panel of Fig. 1. RV variations are clearly visible on different timescales, from a few days to a global trend over the last 3.5 years. This approach allowed us to gather enough data to correctly cover the time series and to average all physical effects such as stellar activity or signals of small planets, leaving only the instrumental systematics.

To illustrate the gain provided by our correction of the systematic instrumental drift, the RV of the constant star HD 185144 is displayed in the bottom panel of Fig. 1. For this target, the RV dispersion decreases from 5.4 to 1.6 m s^{-1} when the RV constant master is subtracted. Figure 2 shows the rms distribution of the 55 stars (including the four reliable constant stars) before and after correction of the RV constant master and illustrates the fact that the SOPHIE RV precision is close to 2 m s^{-1}.

[1] The RV constant master is available upon request.

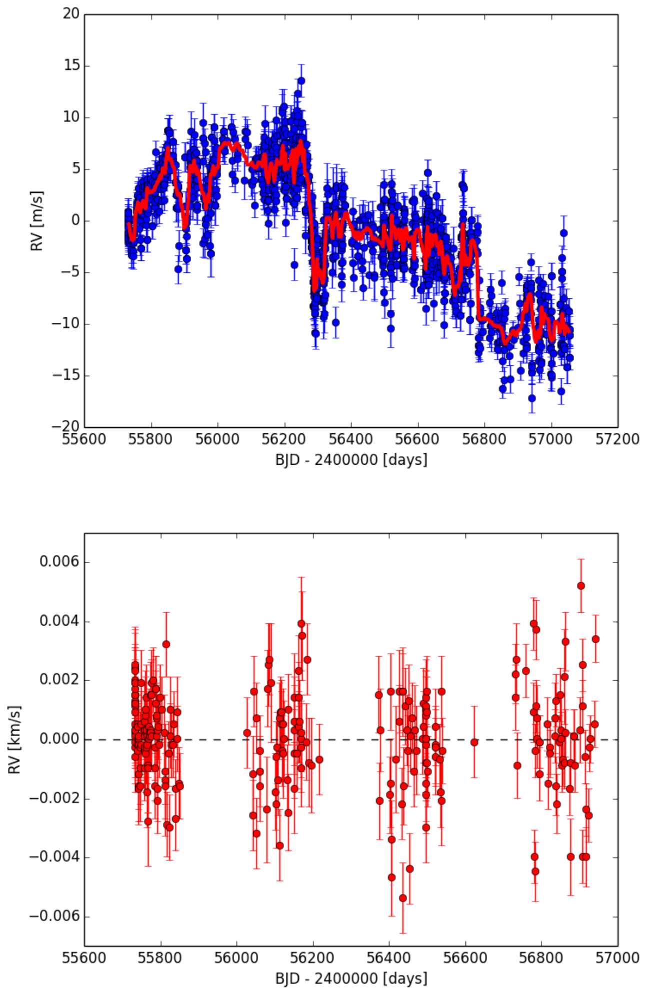

Fig. 1. *Upper panel*: zero-point drift correction (red line) as a function of time and the adjusted RV data set used to create it (blue dots). *Bottom panel*: RV time series of HD 185144 after the zero-point drift correction. This correction decreases the rms from 5.37 m s^{-1} to 1.61 m s^{-1}.

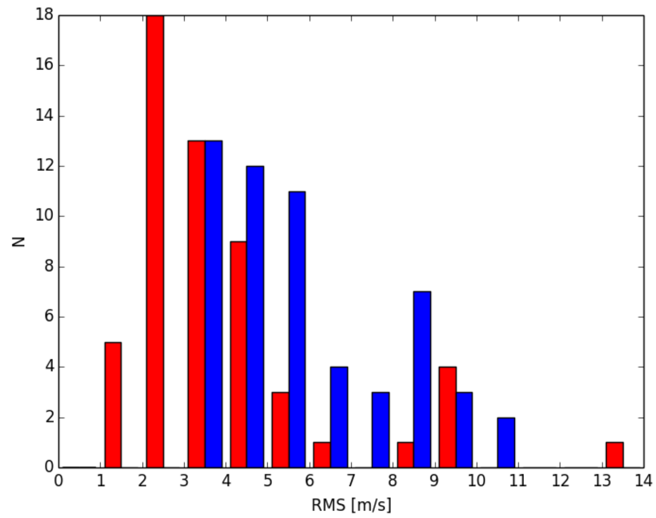

Fig. 2. Initial (blue) and final (red) distribution of the rms in the 55-star sample.

4. Effect on the planetary system HD 190360

4.1. Validation of the correction

To validate the correction of the RV constant master, we analyzed the known planetary system HD 190360 that was observed with SOPHIE in the context of the science validation of the octogonal fibers (Bouchy et al. 2013). The planetary system HD 190360 is composed of a long-period Jupiter (Naef et al. 2003) and a warm Neptune (Vogt et al. 2005). A total of 41 measurements of HD 190360 were gathered with SOPHIE using the same setting as for HD 164595. The radial velocity table is reported in Tables A.1 and A.2. The RV dispersion is 9.5 m s^{-1} and 9.3 m s^{-1} before and after correction of the RV constant master, respectively. The span of our observations was 2.4 years, which is about one-eighth of the period of HD 190360b. This does not allow efficiently constraining the orbital parameters of this planet. We therefore focus our analysis on the warm Neptune HD 190360c.

HD 190360 is a quiet star with a $\log R'_{\rm HK}$ derived from SOPHIE spectra of −5.13. No periodic signals in either the bisector, the CCF-FWHM, or the activity index are present at the two periods found in RVs, which excludes stellar activity as the origin of the Keplerian signals.

To study the impact of our zero point drift correction, we analyzed both the HD 190360 corrected and uncorrected data set with the same methodology. We used the planet analysis and small transit investigation software (PASTIS; Díaz et al. 2014), which is a Bayesian analysis software, for fitting a two-planet model. HD 190360b orbit was not fixed but subjected to strong priors for the Bayesian analysis. Normal distributions were used, centered on the published parameters with widths equal to the published errors in Wright et al. (2009). On the other hand, the other planet parameters were let free, with a Jeffrey distribution for the period, a beta distribution for the eccentricity as defined in Kipping (2013), and uniform distributions for the other parameters. We ran 20 MCMC chains with 300 000 steps each. Only the stationary parts of each chain were kept. The distributions of parameter values of all the remaining uncorrelated chain links then correspond to the target joint posterior-probability distributions for the model parameters.

Table 1 reports our orbital parameters and their uncertainties for both cases. The results are very similar for the two data sets and agree well (within 1σ) with Wright et al. (2009). However, the errors in the uncorrected data are systematically higher (by up to 50%). The dispersion of the residuals is better in the corrected set with 2.1 m s^{-1}, which is consistent with the precision obtained on the constant stars, instead of 3.5 m s^{-1} with the uncorrected data. Moreover, the additional jitter necessary to set the reduced χ^2 to 1 is 1.9 m s^{-1}, instead of 2.9 m s^{-1} for the uncorrected data set. This test demonstrates the relevance of the zero-point drift correction, which significantly improves the quality of the RV data.

4.2. Analysis of the joint HIRES and SOPHIE data

Finally, we combined our data set with the Keck observations used by Wright et al. (2009) to update orbital parameters for the HD 190360 system. 100 MCMC chains of 300 000 steps were run with PASTIS to conduct a global search without a priori for a two-planet fit. The RV time series with our orbital solution is plotted in Fig. 3, and the phase-folded radial velocities for both

Table 1. Comparison of the orbital solutions for HD 190360c with corrected and uncorrected SOPHIE observations.

Parameter	HD 190360c (Uncorrected data)	HD 190360c (Corrected data)
P [days]	17.117 ± 0.015	17.127 ± 0.011
T_0 [BJD]	56149 ± 4	56134 ± 4
e	0.088 ± 0.1	$0.062^{+0.086}_{-0.047}$
ω [deg]	237.1 ± 94	248.5^{+80}_{-210}
K [m s^{-1}]	5.72 ± 0.79	5.64 ± 0.55
$N_{\rm meas}$	41	41
σ (O–C) [m s^{-1}]	2.9	2.1
Jitter (O–C) [m s^{-1}]	3.5	1.9

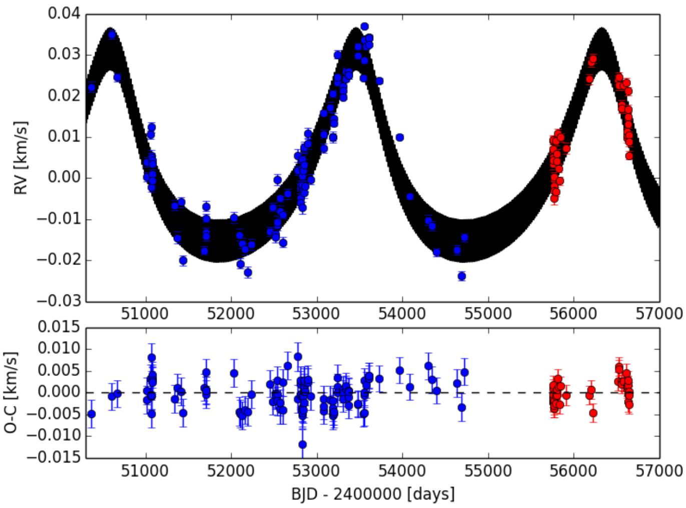

Fig. 3. Radial velocities of HD 190360 for HIRES (blue dots) and SOPHIE (red dots) with the best-fit orbital solution (solid line). Error bars include the photon noise and jitter.

HD 190360b and c are plotted in Fig. 4. The orbital and physical parameters of the two planets are reported in Table 2.

The updated orbital parameters all agree well (within 1σ) or marginally well (within 2σ) with the values previously published in Wright et al. (2009). The precision on all parameters is significantly improved except for the semi-amplitude and ω. Assuming a stellar mass of 0.96 ± 0.1 $M_\odot$ as in Vogt et al. (2005), the minimum mass of HD 190360b and c is 1.50 ± 0.15 $M_{\rm Jup}$ and 20.28 ± 3.16 $M_\oplus$, respectively.

The additional jitter (intrumental and stellar noise) necessary to set the reduced χ^2 to 1 is 2.9 m s^{-1} for HIRES and 1.8 m s^{-1} for SOPHIE. Additionally, the dispersion of the residuals is significantly higher for the HIRES data (3.3 m s^{-1}) than for SOPHIE (2.4 m s^{-1}). To take into account the much longer time span of the Keck observations (11.9 years), we computed the median dispersion of the residuals for all the 2.4 year windows in the HIRES data. Its value is 3.1 m s^{-1}, still significantly higher than for SOPHIE. This could be the result of either a higher instrumental noise or/and a higher stellar jitter at the time of the Keck observations. The latter case seems unlikely since the log $R'_{\rm HK}$ reported in Vogt et al. (2005) is close to our value at −5.09.

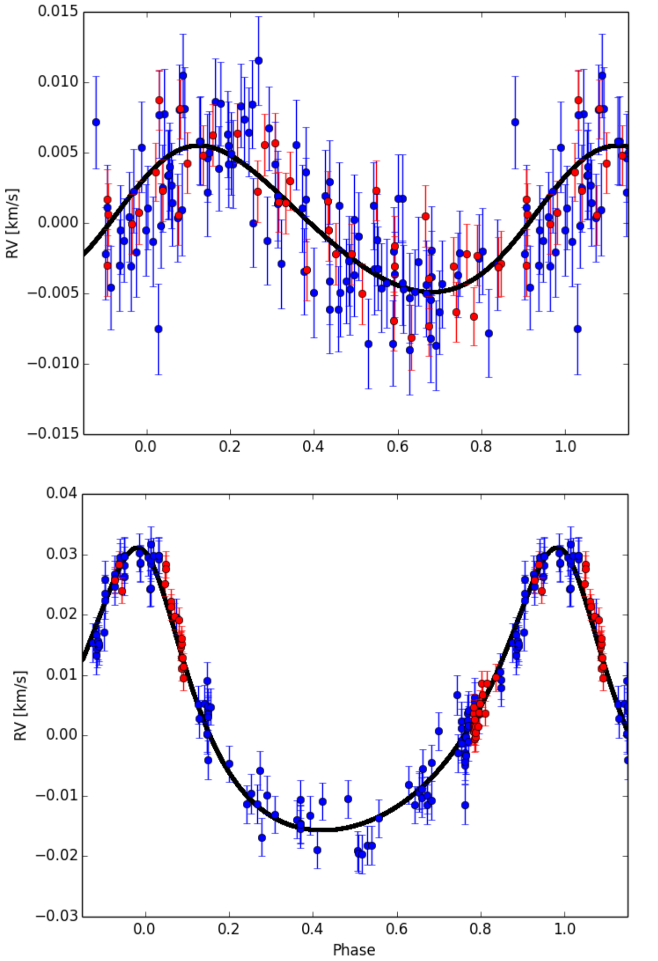

Fig. 4. Phase-folded radial velocities of HD 190360c (*upper panel*) and HD 190360b (*bottom panel*) for HIRES (blue dots) and SOPHIE (red dots) with the best-fit orbital solution (solid line). Error bars include the photon noise and jitter.

Table 2. Updated orbital and physical parameters of HD 190360b and c.

Parameter	HD 190360b	HD 190360c
P [days]	2867.9 ± 7.7	17.1186 ± 0.0016
T_0 [BJD]	59271 ± 19	$55570.3^{+1.5}_{-2.9}$
e	0.343 ± 0.017	0.107 ± 0.07
ω [deg]	14.7 ± 32	305.8^{+39}_{-280}
K [m s^{-1}]	23.39 ± 0.46	5.20 ± 0.37
$m \sin i$ [$M_\oplus$]	475.16 ± 49.0	20.28 ± 3.16
$N_{\rm meas}$ (SOPHIE)	41	
$N_{\rm meas}$ (HIRES)	107	
Jitter (SOPHIE) [m s^{-1}]	1.8	
Jitter (HIRES) [m s^{-1}]	2.9	
σ (O–C) (SOPHIE) [m s^{-1}]	2.4	
σ (O–C) (HIRES) [m s^{-1}]	3.3	

5. HD 164595 data analysis

5.1. Stellar properties

HD 164595 is a G2V star with a magnitude V = 7.08. Its HIPPARCOS parallax (π = 34.57 ± 0.5 mas) implies a distance

Table 3. Observed and inferred stellar parameters for HD 164595.

Parameter	HD 164595	Reference
Spectral type	G2V	HIPPARCOS
π [mas]	34.57 ± 0.5	HIPPARCOS
Distance [pc]	28.93 ± 0.4	HIPPARCOS
V	7.1	HIPPARCOS
$B-V$	0.635	Porto de Mello et al. (2014)
$M_\star$ [$M_\odot$]	0.99 ± 0.03	Porto de Mello et al. (2014)
$T_{\rm eff}$ [K]	5790 ± 40	Porto de Mello et al. (2014)
$\log g$	4.44 ± 0.05	Porto de Mello et al. (2014)
[Fe/H]	−0.04 ± 0.08	Porto de Mello et al. (2014)
$\upsilon \sin i$ [km s^{-1}]	2.1 ± 1	This paper
$\langle\log(R'_{HK})\rangle$	−4.86 ± 0.05	This paper

of 28.93 ± 0.4 pc. This star is considered to be one of the closest known solar analogs. Its parameters were derived by Porto de Mello et al. (2014) in the context of their photometric and spectroscopic survey of solar twin stars within 50 parsecs of the Sun. From the SOPHIE CCFs and using the calibration given by Boisse et al. (2010), we derived a $\upsilon \sin i$ of 2.1 ± 1 km s^{-1}. HD 164595 is known to be a quiet star. Wright et al. (2004) reported a $\log R'_{\rm HK}$ of −5.0 from observations made between 1998 and 2003. More recently, Isaacson & Fischer (2010) reported a slight trend of $\log R'_{\rm HK}$ from −4.97 to −4.86 between 2005 and 2009. Following the method established by Boisse et al. (2010), we derived from our SOPHIE spectra an average value of −4.86 ± 0.05 for $\log R'_{\rm HK}$. Furthermore, computing the median value for each season, we find that the $\log R'_{\rm HK}$ slightly increased from −4.91 in 2012 to −4.88 in 2013 and finally −4.81 in 2014. We also note that the bisector span shows an increasing dispersion over three seasons from 1.7 m s^{-1} in 2012 to 2.0 m s^{-1} in 2013 and finally 3.3 m s^{-1} in 2014. During the last season, the bisector span is marginally correlated with the RV. All these factors seem to indicate that the stellar activity of HD 164595 evolves along a magnetic cycle toward increased activity. Table 3 summarizes the stellar parameters of HD 164595.

5.2. Distinguishing systematic signals and aliases

The Generalized Lomb-Scargle periodogram of the uncorrected radial velocities of HD 164595 is displayed in the upper panel of Fig. 5. A number of significant features appear, the most interesting being a triplet of peaks at 40 ± 5 days. The highest one lies below the 10^{-3} false-alarm probablity (FAP) level. The FAP was calculated with Yorbit (Ségransan et al. 2011) by scrambling the RV data many times and counting the number of randomly generated peaks in the corresponding periodograms with an amplitude higher than the peak of the original set. Here, the 40-day signal of the original data was systematically higher than the peaks of 10 000 scrambled sets. Longer period signals are also found around 120, 180, and 400 days. They are similar to the aliases of the one-year observational period of the spectral window. The middle panel of Fig. 5 shows the periodogram of the RV constant master sampled at the same observing dates as HD 164595. We note that except for the 40-day triplet, other features are the same in the two periodograms. After correction of the systematic drift, that is, after subtracting the constant master RVs from the RVs of HD 164595, the only significant feature in the periodogram (Fig. 5, bottom panel) is the 40-day triplet with a FAP lower than 10^{-5}. This signal is then clearly not introduced by our correction, while other peaks were successfully reduced or removed.

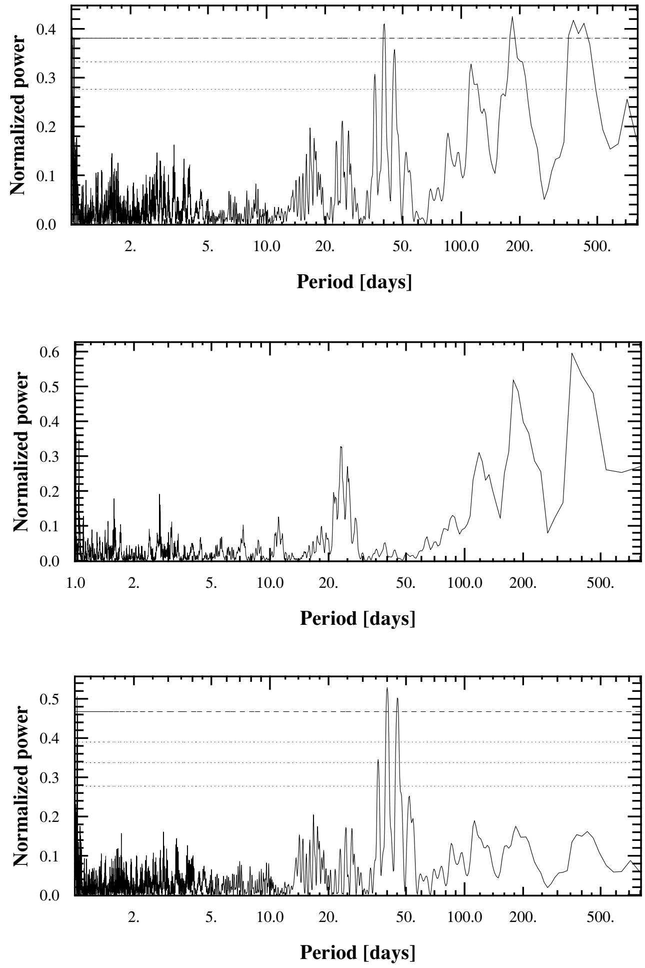

Fig. 5. *Upper panel*: generalized Lomb-Scargle (GLS) periodogram of HD 164595 RV before the constant master correction, with 10^{-3} FAP level (dashed line). *Middle panel*: GLS periodogram of the zero-point drift correction applied to HD 164595 dates of observation. *Bottom panel*: GLS periodogram of the corrected HD 164595 RV data, with 10^{-5} FAP level (dashed line).

The multiplicity of the 40-day feature is due to the convolution with the one-year observational period of the spectral window. The automatic de-aliasing algorithm CLEAN (Roberts et al. 1987) implemented in Yorbit is another way to confirm the unicity of the physical signal in the feature by cleaning up the periodogram. While giving an important diagnostic, this method cannot be used to determinate which frequency is the physical one. This problem is particularly essential for the 40-day and 45-day solutions, which are equally satisfying (with similar amplitudes in the GLS periodogram and a similar $\chi 2$ and residual dispersion for their respective fits).

Dawson & Fabrycky (2010) proposed a method for solving this problem. The concept is to simulate a sinusoidal signal at the period and amplitude of each observational alias and to sample it at the date of observations. By comparing their periodograms, the one that significantly better matches the data periodogram corresponds to the true physical frequency. If the test is inconclusive, it means that the noise prevents identification, and new observations are required. This was the case when we apply this method using only our 66 high-quality observations. We then used our complete data set of 75 measurements (see Fig. 6) and determined that the physical frequency is the 40-day peak.

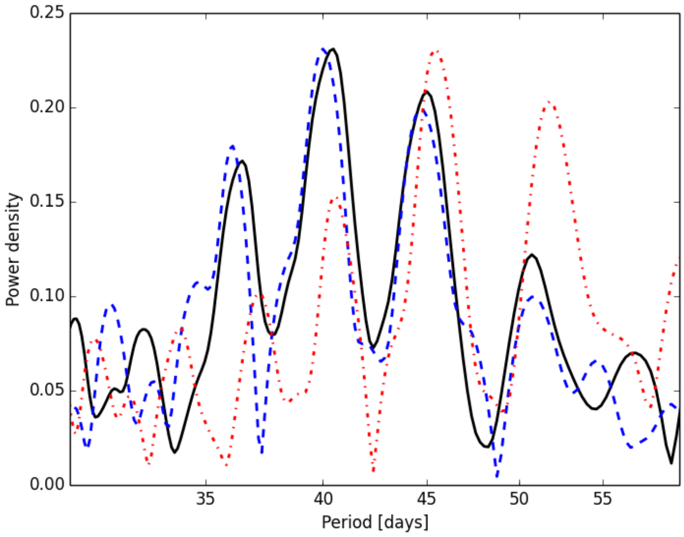

Fig. 6. GLS periodogram of the complete HD 164595 RV data (with all the 75 measurements; solid black curve), the 40-day sinusoid (dashed blue curve) and the 45-day sinusoid (dotted and dashed red curve). The 40-day sinusoid clearly is the best match to the RV data.

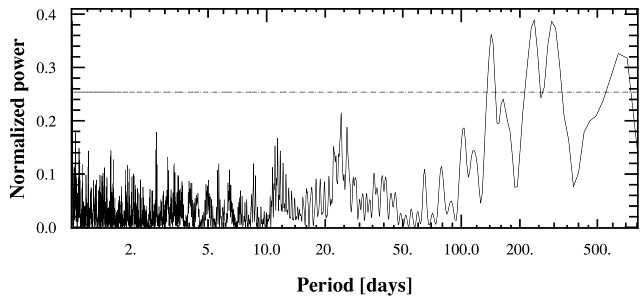

Fig. 7. HD 164595 bisector Generalized Lomb-Scargle periodogram with 0.1 FAP level (dashed line). Long-period signals above this level are caused by a trend in the last season that is marginally correlated with the radial velocities.

5.3. Distinguishing stellar activity

We studied the possibility that the 40-day signal might be due to star-induced activity and correspond to the rotational period. While we noted a slight increase in activity level with time, HD 164595 remained a relatively quiet star even in the last observing season with a $\log R'_{\rm HK}$ below −4.80. Figure 7 shows the periodogram of the bisector span, which can be used to reflect stellar activity. No signal is present at 40 days or at its first harmonics. This also remains true with the FWHM and the $\log R'_{\rm HK}$. There is no correlation between RV and these activity indicators either, except for the already mentioned marginal correlation between RV and the bisector, but only in the last season. Moreover, the rotational period of HD 164595 estimated from the $\log R'_{\rm HK}$ using the calibration published by Mamajek & Hillenbrand (2008) is 20 ± 5 days, which is quite distinct from the observed 40-day signal. We note that no 20-day signal appears in the RV periodogram, which means that the 40-day signal cannot be an observational alias. The HIPPARCOS photometry does not show any significant variations at a level of 13 mmag (with 147 points), and with no hint of periodic signal in the periodogram. We also checked that the 40-day signal maintains the same phase and amplitude over the last two seasons when fitted independantly (the first season does not have enough data points to conclude). We are therefore confident that the 40-day signal is not induced by activity and is planetary in origin.

Table 4. Orbital and physical parameters of HD 164595b.

Parameter	HD 164595b
P [days]	40.00 ± 0.24
T_0 [BJD]	56280 ± 12
e	$0.088^{+0.12}_{-0.066}$
ω [deg]	145^{+160}_{-110}
K [m s^{-1}]	3.05 ± 0.41
$m \sin i$ [$M_\oplus$]	16.14 ± 2.72
a [AU]	0.23
drift [m/s/yr]	−2.34 ± 0.44
$N_{\rm meas}$	66
Data span [days]	809
σ (O–C) [m s^{-1}]	2.3
Jitter [m s^{-1}]	1.8

5.4. Radial-velocity analysis and orbital solution

For the rest of the analysis and the fit of a Keplerian signal we only kept the high-quality data set (66 RV measurements) after removing the nine low-quality measurements (low S/N, moon light contamination, anormal simultaneous thorium-argon flux, see Sect. 2). The rms of the RV time series shown in Fig. 8 (upper panel) is 3.73 m s^{-1}. A slight long-term trend is visible. We used PASTIS to fit a Keplerian and a linear drift to our data without a priori. We ran 20 MCMC chains with 300 000 steps each, and discarded the solutions that did not converge to the 40-day period (some converged to the observational aliases, in particular the 45-day period).

Table 4 reports the orbital parameters and their uncertainties for a Keplerian model with a linear trend, and the best fit is plotted in Fig. 8. The fitted model of the planet has a 40-day period and a semi-amplitude of 3.05 ± 0.41 m s^{-1} with an insignificant eccentricity. Assuming a mass of 0.99 ± 0.03 $M_\odot$ for the star (Porto de Mello et al. 2014), the minimum mass of the planet is 16.1 ± 2.7 $M_\oplus$. With a jitter of 1.8 m s^{-1}, the reduced χ^2 is equal to 1. The residuals after the fit present a dispersion of 2.3 m s^{-1}, and no significant feature appears in the corresponding periodogram. An interesting trend can be observed in the last season. It might correspond to either the activity-related drift that is correlated with the bisector span, or to a shift in the global trend and a subsequent incomplete correction. Trying to correct this trend on the data does not significantly change our reported solution.

Another analysis using the genetic algorithm built into Yorbit (Ségransan et al. 2011) yielded nearly identical parameter values and errors (P = 39.99 ± 0.19 days, K = 2.96 ± 0.40 m s^{-1} and e = 0.078 ± 0.14). We note that the analysis of the uncorrected data does not change our results, but only increases the error bars of our orbital solution, the scatter of the residuals (from 2.2 to 2.9 m s^{-1}), and the corresponding jitter (from 1.8 to 2.7 m s^{-1}).

6. Discussion and conclusion

We have reported the discovery of HD 164595b with the SOPHIE spectrograph. This source is a warm Neptune-like exoplanet with a minimum mass of 16.1 ± 2.7 $M_\oplus$ orbiting a bright

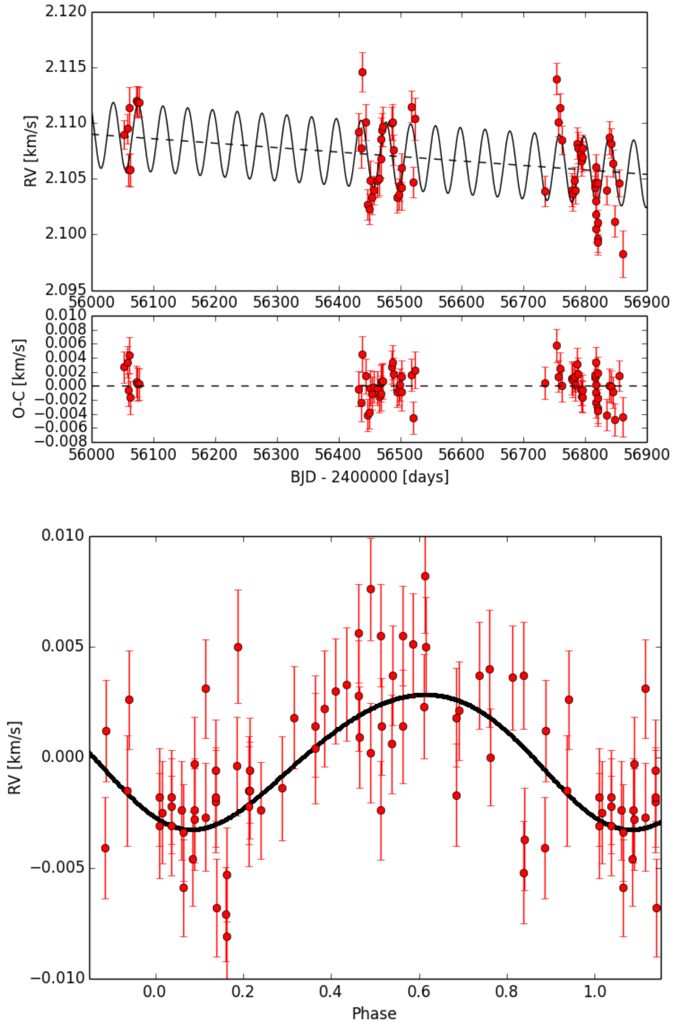

Fig. 8. *Upper panel*: radial velocities of HD 164595 with the best-fit orbital solution (solid line). Error bars include the photon and instrumental noise and the stellar jitter. *Bottom panel*: phase-folded radial velocities of HD 164595 with the best-fit orbital solution (solid line). Error bars include the photon and instrumental noise and the stellar jitter.

solar-analog star with a period of 40.00 ± 0.24 days with no significant eccentricity. An additional long-term RV drift is seen on our data. At this stage, we cannot conclude on its origin. It might be due to a long-period additional companion in the system, but it might likewise be the signature of a stellar magnetic cycle since we observe an slight increase of the activity index over our observing span of 2.2 years. According to Lovis et al. (2011a), a change of 0.1 dex in the $\log R'_{\rm HK}$ may introduce a change of up to 10 m s^{-1} in radial velocity. At this stage, we cannot completely exclude an under-correction of the zero-point drift either. Additional SOPHIE measurements will help to conclude on the long-term drift.

To validate and illustrate the capacity of SOPHIE to reach the 2 m s^{-1} precision thanks to an appropriate correction of systematic instrumental effect, we refined the orbital parameters of the known planetary system HD 190360 based on SOPHIE and HIRES radial velocity measurements. With this precision on all timescales, SOPHIE can detect exoplanets with an RV semi-amplitude as low as 3 m s^{-1}. Nevertheless, pushing the RV precision down to 1 m s^{-1} will be crucial to efficiently cover the parameter space of low-mass exoplanets. Additional improvements are ongoing on SOPHIE, such as the thermal control of

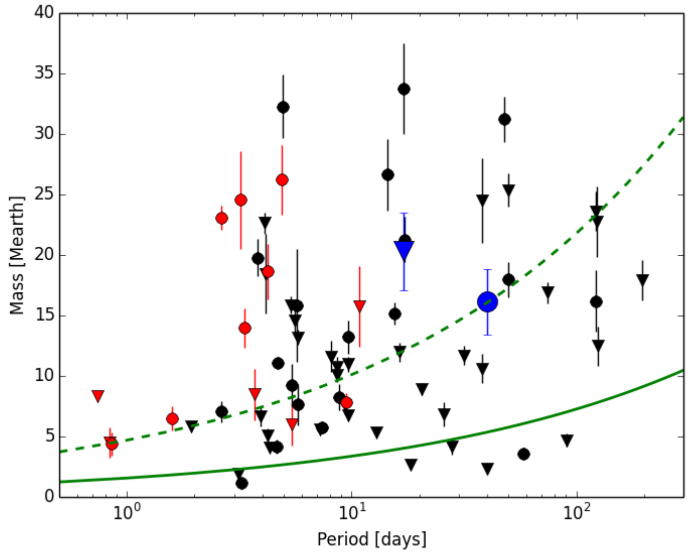

Fig. 9. Mass – orbital period of known planets with $m \sin i < 40\ M_\oplus$, $\Delta m \sin i / m \sin i < 0.3$. Another three planets with $P > 300$ days are not represented because of visibility problems. Transiting planets are shown in red, while the others are black. Triangles correspond to planets in multiplanetary systems. HD 164595b and HD 190360c are the blue circle and triangle. The green curves refer to the 3 m s^{-1} (dashed) and 1 m s^{-1} (solid) iso RV semi-amplitudes for a solar-type star. This diagram is based on data from the exoplanet.org database.

the spectrograph tripod and the implementation of a Fabry-Perot etalon within the calibration unit to improve the determination of the simultaneous drift.

About 70 exoplanets with $m \sin i$ smaller than 40 $M_\oplus$ and an uncertainty on $m \sin i$ smaller than 30% are known. They are displayed in the mass – orbital period diagram in Fig. 9. In that sample, no transiting low-mass planets with period greater than ten days are known except for Kepler-20c (Gautier et al. 2012), which has a period of 10.9 days. Two-thirds of the 18 exoplanets with orbital periods longer than ten days are part of a multiple planetary system. Only three transiting planets with masses in the range 10–20 $M_\oplus$ are known (Kepler-20c, GJ3470b, and HAT-P-26b). Their radii range from 3.1 to 6.3 $R_\oplus$, illustrating the diversity in density of this type of objects. This also underlines the current lack of constraints on these objects. The transition between super-Earths and Neptune-like planets and its dependance on the orbital period is poorly understood. The actual number of planets with precise density measurements is indeed far too low to cover the parameter space and constrain interior, formation, or evolution models for the low-mass planet population. The future transit search missions around bright stars TESS (Ricker et al. 2014) and CHEOPS (Broeg et al. 2013; Fortier et al. 2014) will address this issue from two complementary perspectives. While TESS will substantially increase the number of transiting exoplanets suitable for high-precision RV measurement, CHEOPS will mesure precise radii of known exoplanets that have been discovered with radial velocities to derive precise densities. However, the low overall transit probability of the non-transiting planets of this sample (~300%) implies that CHEOPS will need a significant number of targets at various periods, requiring continuous efforts on low-mass RV surveys.

In this context, HD 164595b is an interesting and potential target for the follow-up transit mission CHEOPS, although its transit probability is only 2%. HD 164595 matches all CHEOPS requirements in terms of coordinates, magnitude, and spectral type. The uncertainty of the transit window extrapolated to 2018 is about six days at this stage, but long-term monitoring of this target with SOPHIE is planned to reduce this uncertainty. Following the mass-radius relation given by Marcy et al. (2014) and assuming that $\sin i = 1$, the expected size of HD 164595b is around 4.7 $R_{\oplus}$. Hence the expected transit probably has a depth close to 1.9 mmag with a duration of 6.1 h. We note, however, that the three transiting planets with similar masses as HD 164595b that were previously mentioned have a radius between 3.1 and 6.3 $R_{\oplus}$. In case of transit, CHEOPS will be fully appropriate to derive the radius with a precision better than 10%. Finally, CHEOPS could also be used to detect transits of additional short-period low-mass companions that are unseen in radial velocities in the HD 164595 system.

Acknowledgements. We gratefully acknowledge the Programme National de Planétologie (telescope time attribution and financial support) of CNRS/INSU, the Swiss National Science Foundation, and the Agence Nationale de la Recherche (grant ANR-08-JCJC-0102-01) for their support. We warmly thank the OHP staff for their great care in optimizing the observations. N.C.S. acknowledges support by Fundação para a Ciência e a Tecnologia (FCT) through Investigador FCT contract of reference IF/00169/2012 and POPH/FSE (EC) by FEDER funding through the program "Programa Operacional de Factores de Competitividade – COMPETE". We further acknowledge FCT through FEDER funds in program COMPETE, as well as through national funds, in the form of the grants with reference RECI/FISAST/0176/2012 (FCOMP-01-0124-FEDER-027493), RECI/FIS-AST/0163/2012 (FCOMP-01-0124-FEDER-027492), and UID/FIS/04434/2013. A.S. is supported by the European Union under a Marie Curie Intra-European Fellowship for Career Development with reference FP7-PEOPLE-2013-IEF, number 627202. P.A.W. acknowledges the support of the French Agence Nationale de la Recherche (ANR), under program ANR-12-BS05-0012 "Exo-Atmos".

References

Baranne, A., Queloz, D., Mayor, M., et al. 1996, A&AS, 119, 373
Beichman, C., Benneke, B., Knutson, H., et al. 2014, PASP, 126, 1134
Boisse, I., Eggenberger, A., Santos, N. C., et al. 2010, A&A, 523, A88
Borucki, W. J., & Koch, D. G. 2011, in IAU Symp. 276, eds. A. Sozzetti, M. G. Lattanzi, & A. P. Boss, 34
Bouchy, F., Hébrard, G., Udry, S., et al. 2009, A&A, 505, 853
Bouchy, F., Díaz, R. F., Hébrard, G., et al. 2013, A&A, 549, A49
Broeg, C., Fortier, A., Ehrenreich, D., et al. 2013, in EPJ Web Conf. 47, 3005
Cosentino, R., Lovis, C., Pepe, F., et al. 2012, in SPIE Conf. Ser., 8446, 84461V
Dawson, R. I., & Fabrycky, D. C. 2010, ApJ, 722, 937
Díaz, R. F., Almenara, J. M., Santerne, A., et al. 2014, MNRAS, 441, 983
Dumusque, X., Pepe, F., Lovis, C., et al. 2012, Nature, 491, 207
Fortier, A., Beck, T., Benz, W., et al. 2014, in SPIE Conf. Ser., 9143, 91432J
Gautier, III, T. N., Charbonneau, D., Rowe, J. F., et al. 2012, ApJ, 749, 15
Howard, A. W., Marcy, G. W., Johnson, J. A., et al. 2010, Science, 330, 653
Howard, A. W., Johnson, J. A., Marcy, G. W., et al. 2011, ApJ, 726, 73
Howard, A. W., Marcy, G. W., Bryson, S. T., et al. 2012, ApJS, 201, 15
Isaacson, H., & Fischer, D. 2010, ApJ, 725, 875
Kipping, D. M. 2013, MNRAS, 434, L51
Lovis, C., Dumusque, X., Santos, N. C., et al. 2011a, unpublished [arXiv:1107.5325]
Lovis, C., Ségransan, D., Mayor, M., et al. 2011b, A&A, 528, A112
Mamajek, E. E., & Hillenbrand, L. A. 2008, ApJ, 687, 1264
Marcy, G. W., Isaacson, H., Howard, A. W., et al. 2014, ApJS, 210, 20
Mayor, M., & Queloz, D. 2012, New Astron. Rev., 56, 19
Mayor, M., Pepe, F., Queloz, D., et al. 2003, The Messenger, 114, 20
Mayor, M., Marmier, M., Lovis, C., et al. 2011, A&A, submitted [arXiv:1109.2497]
Mordasini, C., Alibert, Y., & Benz, W. 2009, A&A, 501, 1139
Mordasini, C., Mayor, M., Udry, S., et al. 2011, A&A, 526, A111
Naef, D., Mayor, M., Korzennik, S. G., et al. 2003, A&A, 410, 1051
Pepe, F., Mayor, M., Galland, F., et al. 2002, A&A, 388, 632
Perruchot, S., Kohler, D., Bouchy, F., et al. 2008, in SPIE Conf. Ser., 7014, 70140J
Perruchot, S., Bouchy, F., Chazelas, B., et al. 2011, in SPIE Conf. Ser., 8151, 15
Porto de Mello, G. F., da Silva, R., da Silva, L., & de Nader, R. V. 2014, A&A, 563, A52
Ricker, G. R., Winn, J. N., Vanderspek, R., et al. 2014, in SPIE Conf. Ser., 9143, 20
Roberts, D. H., Lehar, J., & Dreher, J. W. 1987, AJ, 93, 968
Ségransan, D., Mayor, M., Udry, S., et al. 2011, A&A, 535, A54
Vogt, S. S., Butler, R. P., Marcy, G. W., et al. 2005, ApJ, 632, 638
Wright, J. T., Marcy, G. W., Butler, R. P., & Vogt, S. S. 2004, ApJS, 152, 261
Wright, J. T., Upadhyay, S., Marcy, G. W., et al. 2009, ApJ, 693, 1084

Pages 9 to 10 are available in the electronic edition of the journal at http://www.aanda.org

Appendix A: Radial velocity measurements

Table A.1. Radial-velocity measurements, error bars, and bissector for HD 164595.

BJD	RV [km s^{-1}]	Uncertainty [km s^{-1}]	Biss [km s^{-1}]
56 051.596	2.1088	0.0013	−0.0248
56 058.576	2.1094	0.0013	−0.0240
56 059.487	2.1056	0.0014	−0.0282
56 061.524	2.1112	0.0018	−0.0260
56 062.557	2.1057	0.0015	−0.0285
56 072.524	2.1118	0.0013	−0.0262
56 074.524	2.1118	0.0014	−0.0283
56 076.503	2.1117	0.0013	−0.0295
56 432.514	2.1091	0.0017	−0.0270
56 434.581*	2.1123	0.0014	−0.0270
56 436.544	2.1077	0.0018	−0.0240
56 438.527	2.1145	0.0018	−0.0238
56 443.518	2.1100	0.0016	−0.0288
56 447.595	2.1026	0.0014	−0.0253
56 449.414	2.1022	0.0014	−0.0265
56 451.437	2.1048	0.0017	−0.0273
56 454.408	2.1032	0.0015	−0.0262
56 456.381	2.1039	0.0013	−0.0290
56 462.520	2.1048	0.0016	−0.0262
56 465.499	2.1049	0.0015	−0.0277
56 468.582	2.1067	0.0017	−0.0280
56 469.377	2.1085	0.0019	−0.0290
56 470.421	2.1093	0.0015	−0.0247
56 471.402	2.1095	0.0018	−0.0238
56 486.475	2.1099	0.0015	−0.0290
56 487.540	2.1099	0.0016	−0.0278
56 489.510	2.1075	0.0014	−0.0258
56 495.437	2.1032	0.0013	−0.0280
56 497.549	2.1034	0.0014	−0.0303
56 499.486	2.1042	0.0014	−0.0267
56 501.441	2.1059	0.0013	−0.0262
56 502.480	2.1041	0.0020	−0.0327
56 517.400	2.1114	0.0014	−0.0252
56 520.402*	2.1097	0.0013	−0.0283
56 521.390	2.1045	0.0014	−0.0270
56 524.431	2.1102	0.0019	−0.0288
56 730.676*	2.1143	0.0013	−0.0347
56 733.663*	2.1124	0.0017	−0.0248
56 734.647	2.1037	0.0014	−0.0280
56 753.586	2.1137	0.0014	−0.0258
56 755.611	2.1098	0.0013	−0.0222
56 756.578*	2.1169	0.0023	−0.0287
56 758.605	2.1112	0.0013	−0.0273
56 761.624	2.1082	0.0013	−0.0240
56 777.522	2.1037	0.0015	−0.0283
56 778.570	2.1034	0.0016	−0.0200
56 782.561	2.1047	0.0012	−0.0298
56 783.568	2.1039	0.0012	−0.0313
56 786.585	2.1081	0.0014	−0.0287
56 788.581	2.1076	0.0014	−0.0267
56 792.607	2.1072	0.0014	−0.0288
56 793.555	2.1065	0.0013	−0.0295
56 794.603	2.1078	0.0012	−0.0313
56 795.529	2.1070	0.0013	−0.0342
56 815.447	2.1043	0.0011	−0.0312
56 815.483	2.1046	0.0011	−0.0323
56 816.560	2.1007	0.0012	−0.0323
56 816.592	2.1031	0.0012	−0.0327
56 817.421	2.1020	0.0011	−0.0323
56 817.593	2.1062	0.0011	−0.0282
56 819.464	2.1047	0.0013	−0.0322
56 819.564	2.0997	0.0012	−0.0332
56 820.440	2.0995	0.0011	−0.0310

Notes. The dates with an asterix correspond to low quality data discarded for the analysis.

Table A.1. continued.

BJD	RV [km s^{-1}]	Uncertainty [km s^{-1}]	Biss [km s^{-1}]
56 820.514	2.1013	0.0011	−0.0335
56 834.466	2.1039	0.0013	−0.0295
56 838.411	2.1085	0.0015	−0.0278
56 841.415	2.1080	0.0013	−0.0322
56 844.519	2.1062	0.0012	−0.0313
56 847.487	2.1010	0.0014	−0.0320
56 850.546*	2.0970	0.0016	−0.0363
56 854.401	2.1044	0.0012	−0.0315
56 860.493	2.0982	0.0021	−0.0422
56 900.431*	2.0949	0.0012	−0.0310
56 901.312*	2.1002	0.0013	−0.0317
56 902.312*	2.0951	0.0015	−0.0360

Table A.2. Radial-velocity measurements and error bars for HD 190360 (after correction).

BJD	RV [km s^{-1}]	Uncertainty [km s^{-1}]
55 756.500	−45.2113	0.0013
55 757.487	−45.2097	0.0012
55 758.507	−45.2077	0.0011
55 759.532	−45.2057	0.0012
55 760.522	−45.2055	0.0011
55 761.349	−45.2096	0.0012
55 762.493	−45.2104	0.0011
55 763.380	−45.2151	0.0012
55 765.622	−45.2167	0.0011
55 767.627	−45.2197	0.0014
55 769.479	−45.2178	0.0011
55 772.359	−45.2144	0.0011
55 785.487	−45.2181	0.0011
55 793.383	−45.2056	0.0011
55 796.467	−45.2088	0.0011
55 798.493	−45.2107	0.0012
55 813.428	−45.2038	0.0011
55 818.330	−45.2123	0.0010
55 835.417	−45.2154	0.0010
55 848.299	−45.2048	0.0010
55 908.236	−45.2075	0.0014
56 175.409	−45.1906	0.0012
56 200.333	−45.1865	0.0012
56 220.319	−45.1856	0.0011
56 517.451	−45.1907	0.0011
56 519.428	−45.1901	0.0011
56 521.443	−45.1921	0.0012
56 554.416	−45.1969	0.0011
56 557.378	−45.1977	0.0011
56 583.355	−45.1921	0.0012
56 613.268	−45.1914	0.0011
56 624.292	−45.2050	0.0011
56 625.297	−45.2042	0.0010
56 626.280	−45.2035	0.0011
56 628.290	−45.1997	0.0011
56 629.263	−45.2015	0.0011
56 630.238	−45.1979	0.0010
56 631.246	−45.1935	0.0010
56 638.266	−45.2044	0.0011
56 643.254	−45.2092	0.0010
56 644.242	−45.2058	0.0011